 doi:10.20944/preprints202112.0218.v1

Article

Characterising Penetrometer Tip Contact during Concrete Condition Assessment

Richard Hall[1], Alex Stumpf[1], Avinash Baji[1], Robert Ross[1] Dean Barnett[2]

[1] Department of Engineering, La Trobe University, Melbourne, Australia
[2] Intelligent Water Networks, Victoria, Australia
* Correspondence: R.Ross@latrobe.edu.au; Tel.: +61 438 373 882

Abstract: Concrete condition assessing penetrometers need to be able to distinguish between making contact with a hard (concrete) surface as opposed to a semi-solid (corroded concrete) surface. If a hard surface is mistaken for a soft surface, concrete corrosion may be over-estimated, with the potential for triggering unnecessary remediation works. Unfortunately, the variably-angled surface of a concrete pipe can cause the tip of a force-sensing tactile penetrometer to slip and thus to make this mistake. We investigated whether different shaped tips of a cylindrical penetrometer were better than others at maintaining contact with concrete and not slipping. We designed a range of simple symmetric tip shapes, controlled by a single superellipse parameter. We performed a finite element analysis of these parametric models in SolidWorks before machining in stainless steel. We tested our penetrometer tips on a concrete paver cut to four angles at 20° increments. The results indicate that penetrometers with a squircle-shaped steel tip (a=b=1,n=4) have the least slip, in the context of concrete condition assessment.

Keywords: Concrete, Remote Sensing, Remaining Life Assessment, Condition Assessment

1. Introduction

The worldwide costs for managing millions of kilometres of corroding and deteriorating concrete sewers are tremendous. For example, In 2002, in the United States, the estimated asset loss was $14 billion *per year* [1]. More recently, in 2019, in Germany, the estimated annual replacement cost was $4 billion [2]. Consequently there has been a considerable investment in a range of technologies to assess the condition of concrete sewer (wastewater) pipes [3].

The concrete corrosion in these sewer assets is caused by biogenic hydrogen sulphide produced by the *Acidithiobacillus thiooxidans* sulphide-oxidising micro-organisms [4,5]. The rate of corrosion is non-linear and varies with temperature, pH and environmental factors within the sewer, but can occur quite rapidly with up to 10mm per year previously observed [4]. The crown/obvert region of the pipe has been characterised as the region that suffers most heavily from corrosion [6,7].

Given the potential degraded pipe structural integrity and the high cost of replacement accurate condition assessment becomes a high priority for water authorities. Traditional condition assessment approaches have included: visual (CCTV) acoustic, electrical and electromagnetic [8,9]. Although visual inspection is very useful for some aspects of condition assessment (e.g. crack detection) [10] it is less reliable in detection of corrosion. Likewise, there has been criticism of subjectivity of the other approaches [11] which has led to the extraction of core samples which are drilled out of the pipe [12]. Although it is expensive to perform this core drilling, the structural strength and composition of the samples points to thickness of the remaining un-degraded concrete is an optimum parameter for condition assessment [13]. The slow, expensive and destructive nature of the core drilling operation mean that it is not viable for wide-scale condition assessment. One recent experimental laboratory

Preprints (www.preprints.org) | NOT PEER-REVIEWED | Posted: 13 December 2021 doi:10.20944/preprints202112.0218.v1

technique characterised material hardness (and thereby corrosion) as the resistance as a drill bit makes contact with the surface of the concrete [14].

Previously, we introduced a novel approach to sewer concrete pipe condition assessment using semi-automated penetration testing [15,16], which involves driving an instrumented rod into a material of interest. Penetration testing itself has a long history. In the 1950's the Delft Soil Mechanics Laboratory developed the gold standard for soil testing using a penetrometer with a cone-shaped tip [17]. Over time, penetration testing has come to be seen as a proven, simple, quick and cheap means for in-situ field measurement for a range of applications [18].

The primary advantage of assessing the condition of a concrete surface by touch is that looks can sometimes be deceiving, particularly under variable lighting [19]. On the other hand, the primary disadvantage of assessing the condition of a concrete surface by touch is the need for the touching to be done by a person in a sewer. There are significant risks associated with a person needing to do confined-space entry in a concrete sewer, and the associated occupational health and safety costs can be high enough to preclude wide-scale concrete condition assessment by this means [20]. On the other hand, remote-controlled tools that can touch the concrete, such as a penetrometer, that are safe and relatively cheap to operate, can provide data to assist maintenance planning for urban water infrastructure [21].

For our previous penetrometer [16], we chose to use a 45° conical tip, discounting the option of a flat tip for two reasons. First, that we wanted the tip to pass through the corroded concrete to hard concrete, as opposed to compressing the corroded concrete mix into the solid concrete. Second, we felt that ongoing use of the tip on variably-angled concrete would grind away the flat edge, and potentially introduce some measurement inconsistency depending on the orientation of the device. During field testing however, we observed that the tip skidded, giving false readings, on incident angles greater than 45°. The aim of this paper is therefore to explore the surface contact maintaining capability of other shapes.

This paper is structured as follows. In Section 2 we discuss the design for our penetrometer tips and our analysis of this design in SolidWorks. In Section 3 we discuss our experiments for analysing the behaviour of the penetrometer tip using an Instron 5980 Test Machine. Subsequently, in Section 4 we analysed the results of tip experiment graphs, which show that a squirle-shaped tip maintains the greatest contact over the test set. Finally, we reflect on the degree to which our requirements were met and discuss future directions.

2. Design

In this paper we define tip shape in terms of the superellipse [22], a generalised 2D closed curve equation, with $-a \leq x \leq +a$ and $0 \leq y \leq b$, and $0 \leq n$.

$$|\frac{x}{a}|^n + |\frac{y}{b}|^n = 1$$

Special cases of this equation yield different shapes by modifying a small number of parameters (eg. n), as shown below in Figure 1. Materials analysis can therefore be related to a small number of parameters. We had two shape groups, distinguished only by $b = 1$, see Figure 1, and $b = 2$, see Figure 2, which is an extruded version of the first shape group.

Before milling the tips we performed a Finite Element Analysis (FEA) because we did not want to create tips that were easily destroyed. We modelled using a 250N load using SolidWorks which is the max load force to be applied in our experimental analysis. Figure 3 shows the FEA results at different contact angles, all tips in all configurations were found to be well below the yield stress of the material of 275MPa.

Preprints (www.preprints.org) | NOT PEER-REVIEWED | Posted: 13 December 2021 doi:10.20944/preprints202112.0218.v1

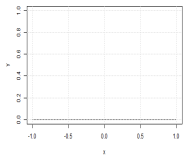

(a) Flat, n=0

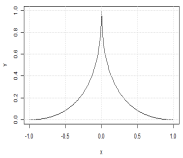

(b) Concave, n=0.5

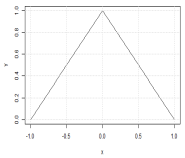

(c) Angled, n=1

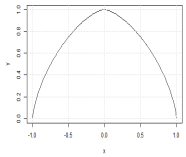

(d) Convex, n=1.5

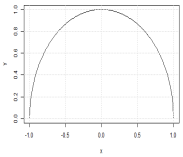

(e) Round, n=2

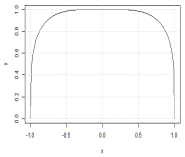

(f) Squircle, n=4

Figure 1. Special case superellipses with $a = b = 1$

3. Experiments

We investigated the ability of our stainless steel penetrometer tips to maintain contact with concrete at different incident angles using an Instron 5980 Test Machine. It was configured to drive the tip with a penetration velocity of 0.1mm per second to record sufficient samples, and to stop driving at 250N detected, below the tensile strength of stainless steel. In order to investigate a reasonable range of incident angles, we waterjet cut a piece of concrete paver aggregate at five incident angle steps (0°, 20°, 40°, 60°, 80°) as shown in Figure 4.

4. Results

We recorded the depth at which the Instron drives the specially-shaped stainless steel tip into the surface of the cut concrete paver before stopping (x axis) against the force required (y axis) to maintain the displacement rate. An example of the ideal behaviour is shown in Figure 5, which is where a 45° angled tip is driven against concrete angled at 0° (flat). Note the plateau of inelastic deformation around 80N, which was visible for sharp tips, less so for rounder tips. The reason that this graph is shown with such a wide horizontal scale is because all results are shown on graphs with the same scale and some results are quite wide.

We now show the results of our experiments for our penetrometer tips, reporting each tip and angle combination. We did multiple measurements for a few tips and found the results similar enough that a single measurement would suffice. In addition, while we cut our concrete paver to five angles, we do not report results on all angles. The results against lower angles (0° and 20°) were similar for all tips. For the majority of these experiments we report against three angles (40°, 60° and 80°). Where angle measurements were excluded it was due to surface geometry making them unsuitable.

For our default *flat* ($n = 0$) tip, Figure 6 shows that it skidded against the 40° concrete around 180N. It also performed relatively poorly against the 80° concrete, skidding past 3mm before maintaining contact, then periodically skidding as the force increased to maximum around an 8mm extension.

For our *basic concave* ($b = 1, n = 0.5$) tip, Figure 7 shows good performance for 40°. Its performance at 60° is not better than the basic concave tip. On the other hand, its performance against 80° is better than the concave tip but worse than the extruded concave tip.

For our *extruded concave* ($b = 2, n = 0.5$) tip, Figure 8 shows a much better performance of this tip against the 80° concrete, as compared to the two previous tips, with a maximum extension of around 5mm. However, the tip performed slightly worse than the basic concave tip against both the 40° and 60° angled pavers.

For our *basic angle* ($b = 1, n = 1$) tip, Figure 9 shows that it ramped up earlier than the flat tip on the 80° concrete, on a similar trajectory to the 60° response around a 2mm extension, however, it then

Preprints (www.preprints.org) | NOT PEER-REVIEWED | Posted: 13 December 2021 doi:10.20944/preprints202112.0218.v1

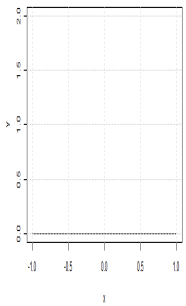

(a) Flat, n=0

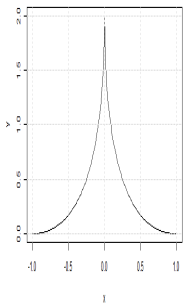

(b) Concave, n=0.5

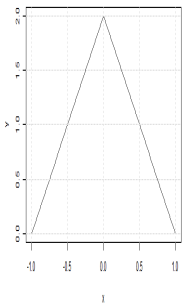

(c) Angled, n=1

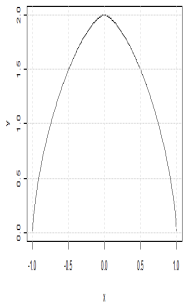

(d) Convex, n=1.5

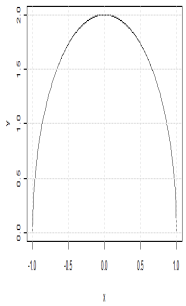

(e) Round, n=2

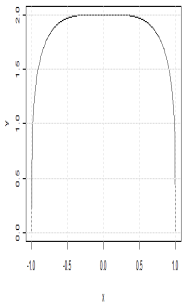

(f) Squircle, n=4

Figure 2. Special case superellipses with $a = 1, b = 2$

responded much more wildly than the flat tip and extended further. It also skidded against the 40° concrete at a higher force than the flat tip.

For our *extruded angle* ($b = 2, n = 1$) tip, Figure 10 shows that it performed no better than the basic angle tip. Against the 80° concrete it ramps up at a similar point, but it has a considerably larger final extension.

For our *basic convex* ($b = 1, n = 1.5$) tip, Figure 11 shows reasonable performance against 40° and 60° concrete. There is a slightly greater extension than the extruded angle tip against the 80° concrete, there are a few larger troughs before the force climbs vertically.

For our *extruded convex* ($b = 2, n = 1.5$) tip, Figure 12 shows that it performs about the same as the basic convex tip against 40° and 60° concrete. At first glance it appears to perform significantly worse against 80° concrete, given the long wild tail. However it does ramp up to around 50N much earlier than most of the previous tips except for the basic concave tip.

For our *basic round* ($b = 1, n = 2$) tip, Figure 13 shows a very similar performance to the basic convex tip.

Preprints (www.preprints.org) | NOT PEER-REVIEWED | Posted: 13 December 2021 doi:10.20944/preprints202112.0218.v1

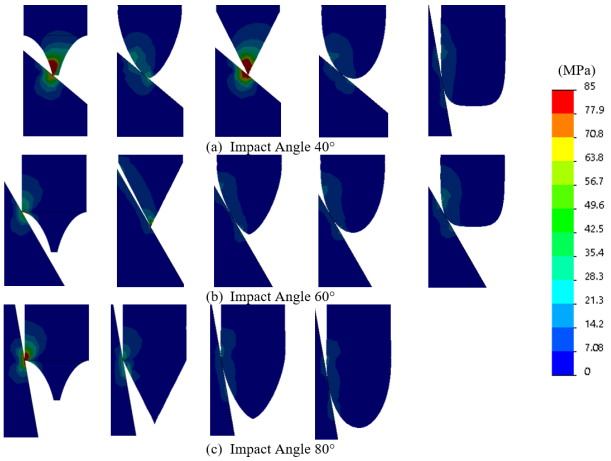

Figure 3. Tip FEA Analysis

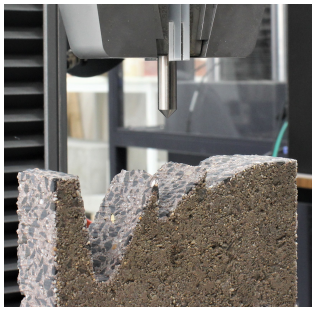

Figure 4. A photo of the Instron driving a tip against concrete

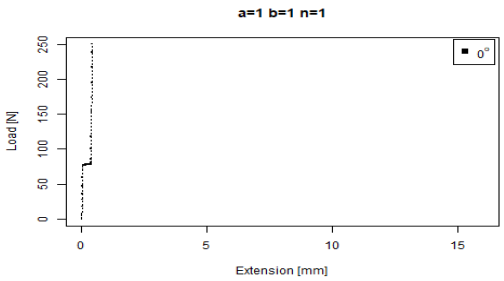

Figure 5. Angled tip with $a = 1, b = 1, n = 1$

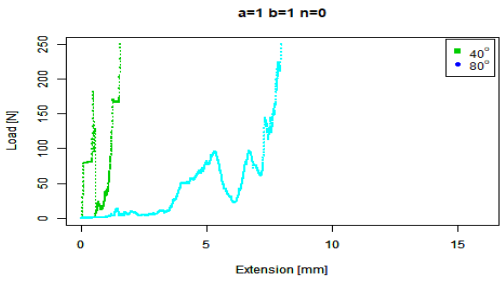

Figure 6. Flat tip

For our *extruded round* ($b = 2, n = 2$) tip, Figure 14 shows that it performs similarly to the extruded convex tip, except its performance against 60° concrete is more similar to its performance against 40° concrete.

Preprints (www.preprints.org) | NOT PEER-REVIEWED | Posted: 13 December 2021 doi:10.20944/preprints202112.0218.v1

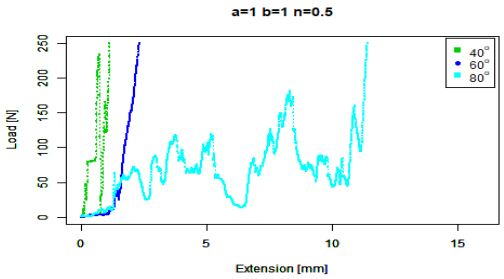

Figure 7. Basic concave tip

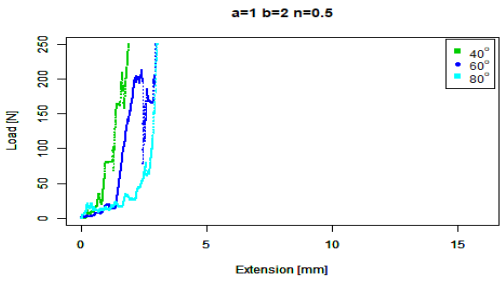

Figure 8. Extruded concave tip

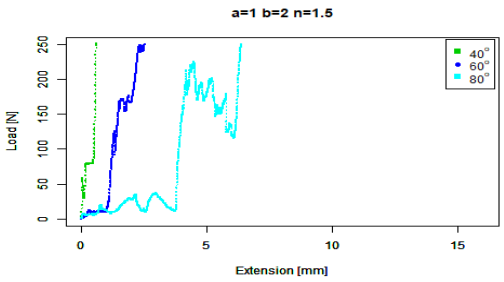

Figure 9. Basic angled tip

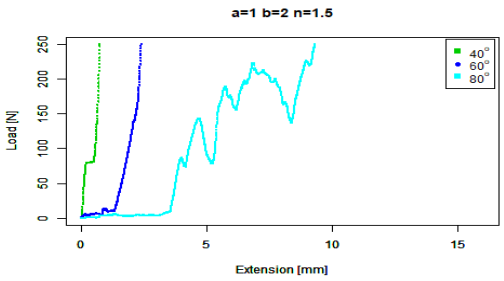

Figure 10. Extruded angle tip

For our *basic squircle* ($b = 1, n = 4$) tip, Figure 15 shows similar performance to the basic convex tip against 40° concrete. It also shows similar performance to the extruded round tip against 60° concrete. However, the gradient of its performance against 80° concrete is the steepest of all the tips, however it slips above 200N.

For our *extruded squircle* ($b = 2, n = 4$) tip, Figure 16 shows that it performs similarly to the basic squircle with a steep starting ramp except that its length before slipping is shorter.

These eleven graphs show much more similar performance by the tips against the 40° and 60° than against the 80° concrete. In Figure 17 we now compare the better performers against 80° with a much smaller horizontal scale, prioritising tips that have a steeper initial gradient from zero (eg. Figure

Preprints (www.preprints.org) | NOT PEER-REVIEWED | Posted: 13 December 2021 doi:10.20944/preprints202112.0218.v1

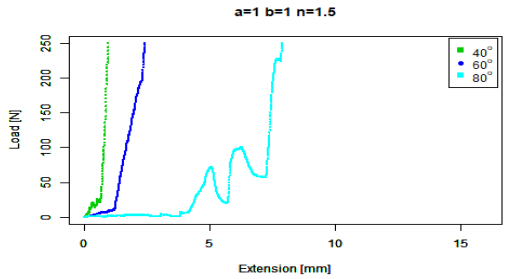

Figure 11. Basic convex tip

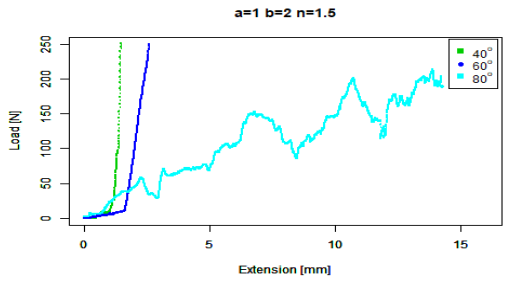

Figure 12. Extruded convex tip

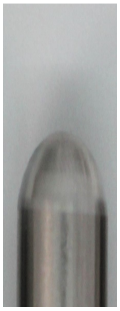

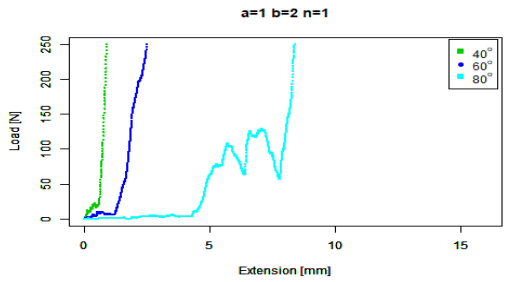

Figure 13. Basic round tip

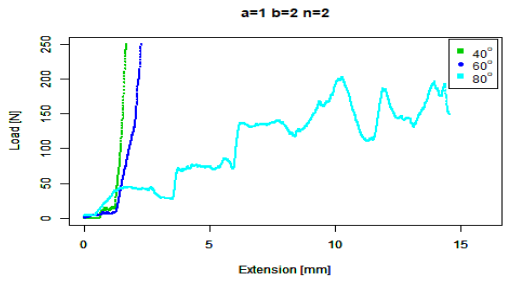

Figure 14. Extruded round tip

16 over tips which have a flatter initial gradient (eg. Figure 13). A steeper gradient can be identified faster by a force sensing device in comparison to a flatter gradient. Note that the colours no longer correspond with angles.

Figure 17 shows that the extruded tips performed better overall than the basic tips with steeper response gradients. The *extruded concave* tip (black) starts with the steepest gradient both at the start and particularly around a extension of 3mm. However the middle section from approximately 0.1mm to 2.8mm has a lower gradient which is also bumpier than the three other curves. The *extruded squircle* tip has the second steepest early gradient (dark blue), which rises above 50N at a 1mm extension but then slips below 50N at 3mm, behaving similarly and better than the extruded round tip (light green).

Preprints (www.preprints.org) | NOT PEER-REVIEWED | Posted: 13 December 2021 doi:10.20944/preprints202112.0218.v1

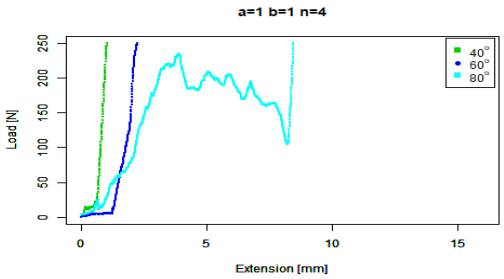

Figure 15. Basic squircle tip

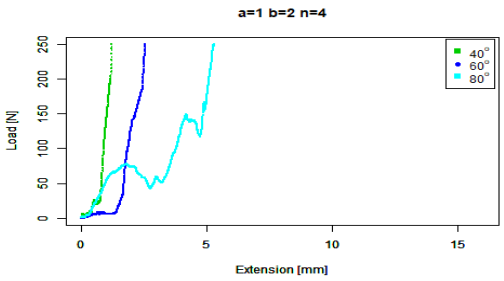

Figure 16. Extruded squircle tip

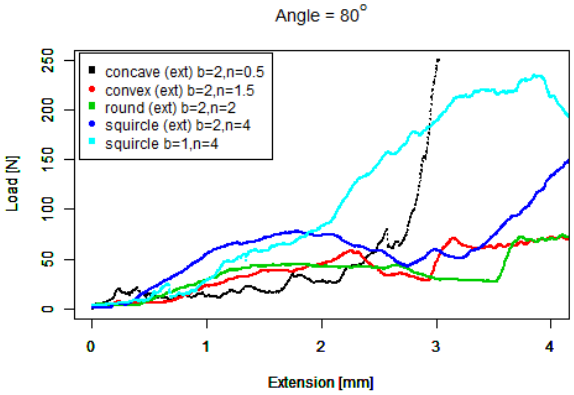

Figure 17. Steeper gradients against 80°

The *squircle* tip (light blue) exceeds 50N second and climbs with minor slips until it crosses the *extruded concave* (black) tip around 3mm but slips above 200N.

Figure 18 shows that three tips converge first around 50N, the *squircle, concave*, and *round* tips. The *extruded squircle* and *extruded convex* tips then have the next best performance, with reasonably similar paths. The data is similar to the 80° data in that the *squircle* grips better than the *extruded squircle*.

5. Conclusion

A simple parameterised representation of penetrometer tip shape was introduced, and the ability of our shaped-as-X steel tips to maintain indentation contact with concrete at different incident angles was investigated.

While our modelling of the concave tip suggested that it would be fragile, in the laboratory setting it did not break against the concrete at any angle, and performed quite competitively against the higher angles. However, in deploying in a field environment, we would prefer not to use this tip for two reasons: we believed that it is more likely to break, and because a sharp tip potentially creates a safety hazard.

Preprints (www.preprints.org) | NOT PEER-REVIEWED | Posted: 13 December 2021 doi:10.20944/preprints202112.0218.v1

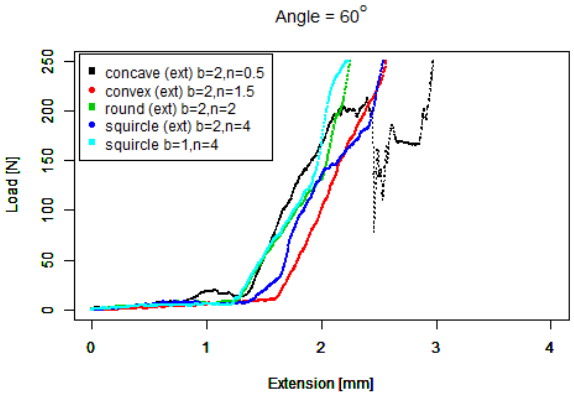

Figure 18. Steeper gradients against 60°

Consequently, we selected the basic squircle (a=1,b=1,n=4) as the best performer at maintaining surface contact through its changing curvature. In terms of selecting a force sensor to detect a solid surface, we chose a force sensor rated at 50N, which gives us a maximum overextension of up to 2mm. We plan to investigate other parameters such as material and shape complexity to further improve our penetrometer design.

Author Contributions: Conceptualization, Richard Hall, Alex Stumpf, Avinash Baji, Robert Ross; Formal analysis, Alex Stumpf, Avinash Baji; Funding acquisition, Robert Ross, Dean Barnett; Investigation, Richard Hall, Alex Stumpf, Avinash Baji, Robert Ross; Methodology,Richard Hall, Alex Stumpf, Avinash Baji, Robert Ross, Dean Barnett; Project administration, Robert Ross and Richard Hall; Writing – original draft, Robert Ross and Richard Hall.

Funding: This research was funded by Intelligent Water Networks (IWN).

References

1. Brongers, M.; Virmani, P.; Payer, J. Drinking water and sewer systems in corrosion costs and preventative strategies in the United States. *United States Department of Transportation Federal Highway Administration* **2002**.
2. Tscheikner-Gratl, F.; Caradot, N.; Cherqui, F.; Leitão, J.P.; Ahmadi, M.; Langeveld, J.G.; Le Gat, Y.; Scholten, L.; Roghani, B.; Rodríguez, J.P.; others. Sewer asset management–state of the art and research needs. *Urban Water Journal* **2019**, *16*, 662–675.
3. Selvakumar, A.; Tuccillo, M.E.; Martel, K.D.; Matthews, J.C.; Feeney, C. Demonstration and evaluation of state-of-the-art wastewater collection systems condition assessment technologies. *Journal of Pipeline Systems Engineering and Practice* **2014**, *5*, 04013018.
4. Vollertsen, J.; Nielsen, A.H.; Jensen, H.S.; Wium-Andersen, T.; Hvitved-Jacobsen, T. Corrosion of concrete sewers—the kinetics of hydrogen sulfide oxidation. *Science of the total environment* **2008**, *394*, 162–170.
5. Parker, C. THE CORROSION OF CONCRETE: 2. THE FUNCTION OF THIOBACILLUS CONCRETIVORUS (NOV. SPEC.) IN THE CORROSION OF CONCRETE EXPOSED TO ATMOSPHERES CONTAINING HYDROGEN SULPHIDE. *Australian Journal of Experimental Biology and Medical Science* **1945**, *23*, 91–98.
6. Islander, R.L.; Devinny, J.S.; Mansfeld, F.; Postyn, A.; Shih, H. Microbial ecology of crown corrosion in sewers. *Journal of Environmental Engineering* **1991**, *117*, 751–770.
7. Sydney, R.; Esfandi, E.; Surapaneni, S. Control concrete sewer corrosion via the crown spray process. *Water environment research* **1996**, *68*, 338–347.
8. Lai, F.; Feeney, C. Condition Assessment of Wastewater Collection Systems. Proceedings of the EPA Science Forum, 2008.
9. Liu, Z.; Kleiner, Y. State of the art review of inspection technologies for condition assessment of water pipes. *Measurement* **2013**, *46*, 1–15.

10. Huynh, P.; Ross, R.; Martchenko, A.; Devlin, J. Dou-edge evaluation algorithm for automatic thin crack detection in pipelines. 2015 IEEE International Conference on Signal and Image Processing Applications (ICSIPA). IEEE, 2015, pp. 191–196.
11. Dirksen, J.; Clemens, F.; Korving, H.; Cherqui, F.; Le Gauffre, P.; Ertl, T.; Plihal, H.; Müller, K.; Snaterse, C. The consistency of visual sewer inspection data. *Structure and Infrastructure Engineering* **2013**, *9*, 214–228.
12. Stanić, N.; De Haan, C.; Tirion, M.; Langeveld, J.; Clemens, F. Comparison of core sampling and visual inspection for assessment of concrete sewer pipe condition. *Water science and technology* **2013**, *67*, 2458–2466.
13. Stanić, N.; Langeveld, J.; Salet, T.; Clemens, F. Relating the structural strength of concrete sewer pipes and material properties retrieved from core samples. *Structure and Infrastructure Engineering* **2017**, *13*, 637–651.
14. Giovanangeli, N.; Piyathilaka, L.; Kodagoda, S.; Thiyagarajan, K.; Barclay, S.; Vitanage, D. Design and development of drill-resistance sensor technology for accurately measuring microbiologically corroded concrete depths. ISARC. Proceedings of the International Symposium on Automation and Robotics in Construction. IAARC Publications, 2019, Vol. 36, pp. 735–742.
15. Ross, R.; Baji, A.; Barnett, D. Inner Profile Measurement for Pipes Using Penetration Testing. *Sensors* **2019**, *19*, 237.
16. Ross, R.; Stumpf, A.; Barnett, D.; Hall, R. Condition assessment for concrete sewer pipes using displacement probes: a robotic design case study. *Robotics* **2021**, *10*, 64.
17. Massarsch, K. Cone penetration testing—a historic perspective. Proceedings 3rd international symposium on cone penetration testing. Las Vegas, Nevada, USA, 2014, pp. 13–14.
18. Perumpral, J. Cone penetrometer applications—A review. *Transactions of the ASAE* **1987**, *30*, 939–0944.
19. Koch, C.; Georgieva, K.; Kasireddy, V.; Akinci, B.; Fieguth, P. A review on computer vision based defect detection and condition assessment of concrete and asphalt civil infrastructure. *Advanced Engineering Informatics* **2015**, *29*, 196–210.
20. Garda, A.; Castillo, F.; Binet, G.; Litrico, X.; Gil, A. Needs and potential of unmanned vehicles in sewers. *La Houille Blanche* **2016**, pp. 24–29.
21. Baah, K.; Dubey, B.; Harvey, R.; McBean, E. A risk-based approach to sanitary sewer pipe asset management. *Science of the Total Environment* **2015**, *505*, 1011–1017.
22. Gardiner, M. The superellipse: a curve that lies between the ellipse and the rectangle. *Scientific American* **1965**, *213*, 222–232.